Successive weak-ferromagnetic transitions in α-Sm2S3

Successive weak-ferromagnetic transitions in α-Sm_2S_3

L. J. Zhao and S. Ebisu*

Division of Applied Sciences, Muroran Institute of Technology, 27-1, Mizumoto-cho, Muroran, 050-8585, Japan

* Corresponding author.

E-mail address: ebisu@mmm.muroran-it.ac.jp (S. Ebisu)

Abstract

Magnetization and specific heat have been investigated for a single crystal and a sintered sample of α-Sm_2S_3 having an orthorhombic crystal structure. The weak-ferromagnetic transitions have been found and the Curie temperatures are determined as T_{C1} = 3.6 K and T_{C2} = 1.8 K from the magnetic specific heat $C_{mag}(T)$ of a single crystal under no magnetic field. The weak-ferromagnetic features are extremely anisotropic, and the easy-magnetization axis is ***c*** which is perpendicular to the longitudinal direction of the needle-like single crystal. The saturation magnetization at T = 2.0 K and $\boldsymbol{H}$ = 100 Oe along the ***c***-axis after field-cooling (FC) is so small as 1/18 of the full moment of Sm^{3+}. The magnetization $M(T)$ after zero-field cooling (ZFC) shows a curious peak at about 4.5 K just above T_{C1} regardless of the direction of the applied magnetic field for the single crystal. While both $M(T)$ curves of FC/ZFC for the sintered sample show such peaks at about 4.0 K. The $C_{mag}(T)$ behaves characteristically depending on the direction of the applied magnetic field. The magnetic entropy $S_{mag}(T)$ is also extremely anisotropic for the magnetic-field direction, and the $S_{mag}(T)$ under $\boldsymbol{H}$//***a*** is almost invariant to the field within 70 kOe. Therefore, it might be useable for controlling MCE effect by its rotating in magnetic field.

Keywords: Rare-earth sesquisulfides, Successive weak-ferromagnetic transitions, Strong anisotropy, Zero-field-cooling, MCE effect

Introduction

Rare-earth sulfides have received much attention owing to their varied physical properties and a large number of works have been performed on binary rare-earth sulfides over the last decades. In particular, there are many studies on rare-earth sesquisulfides because of their diversity of structural types and their interesting physical properties [1-12]. Among them, alpha-type rare earth sesquisulfides α-R_2S_3 (R = La-Dy, except Pm and Eu) have attracted considerable interest for their novel physical properties related to magnetic transitions in recent years [13-29].

The α-R_2S_3 compounds possess an orthorhombic crystal structure with the space group *Pnma*, which has two independent rare earth sites labeled $R1$ and $R2$, as shown in Fig. 1. For clearly seen, sulfur atoms are not shown here. The $R1$ atoms form planes with buckling in the *ab*-plane and the $R2$ atoms are connected to these planes. The decorated planes are stacked along the ***c***-axis. Here the atoms connected by dashed lines are on (0 1/4 0) plane and the atoms connected by solid lines are on (0 3/4 0) plane. The complicated physical properties in α-R_2S_3 compounds have been considered to result from the competition and coexistence of the various magnetic interactions among rare earth sites.

Novel physical properties of nearly all α-R_2S_3 compounds have been investigated by our groups from 2004 [13-17, 19-29]. These compounds except α-Gd_2S_3 show successive magnetic transitions at lower temperatures, and curious physical properties around the transition temperatures. As for α-Gd_2S_3, it has only one antiferromagnetic (AFM) transition at T_N = 9.9 K with large anisotropic behavior [14-18]. The results of neutron diffraction of α-Gd_2S_3 reveal that the magnetic unit cell of α-Gd_2S_3 below T_N was the same as the chemical unit cell [17]. Large entropy just above T_N calculated from magnetic specific heat is about $2R\ln 8$, which shows all Gd moments on both sites of Gd1 and Gd2 order at T_N simultaneously [15]. Also, in the case of α-Pr_2S_3, we have observed only one peak in the temperature dependence of the specific heat corresponding to a phase transition. However, the specific heat demonstrates a tendency to rise with decreasing temperature below 1 K. They have concluded that α-Pr_2S_3 shows successive AFM transitions at T_{N1}

= 2.95 K and T_{N1} < 0.4 K [13]. For the other compounds of α-R_2S_3 (R = Nd [13], Tb [24-27] and Dy [19-27]), successive AFM transitions were found at T_{N1} = 2.75 K / T_{N2} = 0.65 K for α-Nd_2S_3, at 12.5 K / 3.5 K for α-Tb_2S_3 and at 11.4 K / 6.4 K for α-Dy_2S_3, respectively. In addition, it has been confirmed by neutron diffraction measurement for α-Tb_2S_3 that the magnetic moments on Tb1 and Tb2 sites order at T_{N1} and T_{N2}, respectively [25].

Only in the case of α-Sm_2S_3, successive weak ferromagnetic (WFM) transitions have been found. However, the maximum value of the magnetization at 100 Oe of applied magnetic field is so small as 7.7 % of full saturation moment of Sm^{3+} [28]. Such novel magnetic property different from the series of α-R_2S_3 compounds is noteworthy.

Furthermore, extremely rare behavior of the electrical resistivity in the single crystals of α-Dy_2S_3 and α-Sm_2S_3 has been found [19, 28, 29]. In both of them, the electrical resistivity shows an enormous increase and decreases rapidly in the narrow temperature region near the magnetic phase transition temperatures under no magnetic field. After applying magnetic field, such enormous changes were suppressed strongly [19, 28]. The suppression effect is also anisotropic in the *ac*-plane for an applied magnetic field along the easy magnetization axis and hard magnetization axis in both α-Dy_2S_3 and α-Sm_2S_3 [29].

In the present work, we have successfully grown single crystals of α-Sm_2S_3 and prepared the sintered sample with a single-phase. This paper focuses on the anomalous behavior of α-Sm_2S_3 in the temperature dependence of magnetization and specific heat. The features of successive weak-ferromagnetic transitions and strong anisotropy were found in magnetization. Behavior of the specific-heat peaks strongly depending on the direction of the applied magnetic field was also found. The above-mentioned phenomena were discussed in detail in this paper.

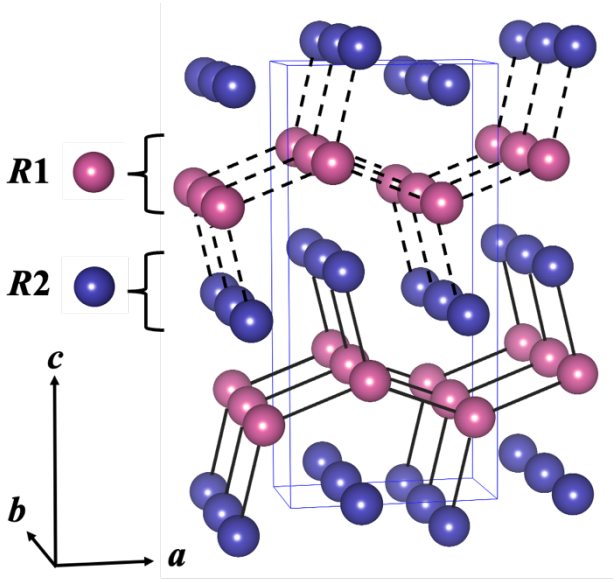

Fig. 1 The crystal structure of α-R_2S_3 compound, in which sulfur atoms are not shown for clarity. The two crystallographically independent rare earth sites are shown as R1 and R2. The rectangular parallelepiped is a unit cell.

2. Experimental

The powder sample of polycrystalline α-Sm_2S_3 used in this study was synthesized by the sulfurization method. The powder of Sm_2O_3 (99.9%) was heated in an alumina boat at 1273 K for 5 h under the flow of the Ar gas containing CS_2 [14, 30]. Single crystals of α-Sm_2S_3 were grown by a chemical transport reaction method using iodine as a carrier. The detailed experimental process can be found in Ref. [14, 31-33]. The sintered sample was prepared as follows; the powder of α-Sm_2S_3 polycrystalline was compressed in a rectangular bar (2 mm × 10 mm × 0.34 mm) under about 180 MPa and then sintered at 1273 K for 24 h in the same atmosphere as sulfurization.

Identification of the powder sample and determination of the crystal-plane orientation of the single crystal were made by X-ray diffraction (XRD) method (Rigaku Corp.) using Cu K_α radiation (λ = 1.5406 Å).

Temperature dependence of the DC magnetization $M(T)$ was measured using a superconducting quantum interference device (SQUID) magnetometer (MPMS, Quantum Design). The $M(T)$ of a single crystal and a sintered sample were measured in two type processes, namely, zero-field-

cooling (ZFC) and field-cooling (FC) in the temperature range of 2-10 K under the various applied magnetic fields within 20 kOe (single crystal) / 70 kOe (sintered sample).

Temperature dependence of specific heat $C(T)$ was measured by a relaxation method using Physical Property Measurement System (PPMS, Quantum Design). The $C(T)$ of a single crystal and a sintered sample were measured in the temperature range of 0.4-300 K (or 15 K) in the absence of a magnetic field and the presence of various magnetic fields within 70 kOe. For a single crystal, the magnetic field $\boldsymbol{H}$ in both $M(T)$ and $C(T)$ measurements was applied in three directions, namely, $\boldsymbol{H}$ parallel to each crystal axis $\boldsymbol{a}$, $\boldsymbol{b}$ and $\boldsymbol{c}$.

3. Results and discussion

3.1 Sample preparation and X-ray diffraction measurements

Figure 2(a) shows XRD patterns of powder sample just after sulfurizing and powder sample crushed from sintered bars for α-Sm_2S_3. All the peaks were assigned to α-Sm_2S_3 single phase having an orthorhombic crystal structure with the space group *Pnma*. The lattice parameters evaluated are almost the same as a = 7.379 Å, b = 3.973 Å, c = 15.377 Å for the former and a = 7.380 Å, b = 3.973 Å, c = 15.373 Å for the latter. Both XRD patterns agree well, and the difference of the lattice parameters between the samples are less than 0.03% being within experimental error. Therefore, we believe that these samples are essentially the same.

The single crystal used in this study is needle-shaped and has a hexagonal cross-section perpendicular to the $\boldsymbol{b}$-axis (longer direction of a needle). The six-side plane orientations of the single crystal were determined as two (001) planes and four (101) planes by the XRD method, as shown in Fig. 2(b).

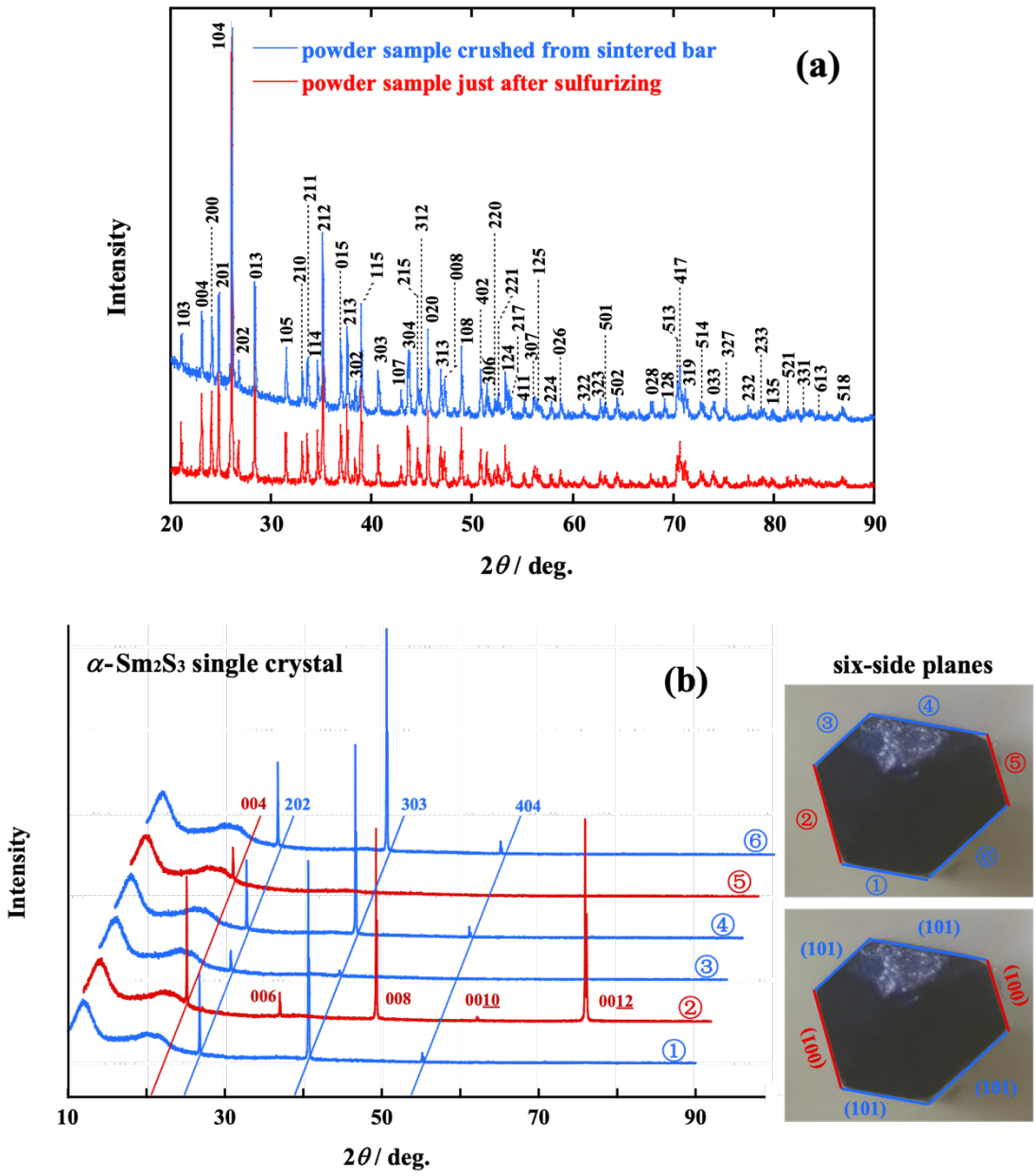

Fig. 2 XRD patterns of α-Sm_2S_3 compound: (a) for powder sample just after sulfurizing and powder sample crushed from sintered bar; (b) for six-side planes perpendicular to the ***b***-axis of a single crystal.

3.2 Magnetic properties

The temperature dependence of magnetization, $M(T)$, for a single crystal of α-Sm_2S_3 in an applied magnetic field of 100 Oe along each crystal axis is shown in Fig. 3(a)-(c). The temperature dependence is rather weak in the range of $T > 5$ K. For a single crystal, while decreasing

temperature, all the $M(T)$ for FC show abrupt rising below 5 K and then show a shoulder around 3.8 K followed by another increase at lower temperatures. The abrupt rising seems to be a feature of ferromagnetic (FM) transition. However, the value of the magnetization is so small even in the case of $\boldsymbol{H}//\boldsymbol{c}$. There exists strong magnetic anisotropy among directions of the crystal axes ($\boldsymbol{a}$, $\boldsymbol{b}$ and $\boldsymbol{c}$) and the $\boldsymbol{c}$-axis is the easy-magnetization axis in the low temperature range near the transition temperature. The value of M_c (magnetization for $\boldsymbol{H}//\boldsymbol{c}$) at 2 K is 0.04 μ_B, which is about 1/18 of full saturation moment 0.71 μ_B for trivalent Samarium (Sm^{3+}) and slightly smaller than the previous report [28] owing to sample dependence. However, on the other hand, the values of M_c are about 20 times larger than those of M_b and M_a in the lower temperatures. Such WFM property in the α-Sm_2S_3 is considered to be brought about by the small FM contribution originating from the Sm^{3+} canted moments. Furthermore, the magnetic moment of Sm^{3+} itself is small due to energy level splitting for Sm^{3+} caused by crystalline electric field. We will call this small FM contribution "net moment" from now on. Next let us see the ZFC curves. Sharp peaks are observed in ZFC $M(T)$ curves at 4.4 K for $\boldsymbol{H}//\boldsymbol{c}$ and at 4.5 K for $\boldsymbol{H}//\boldsymbol{a}$ and $\boldsymbol{H}//\boldsymbol{b}$. Such a distinct behavior between FC/ZFC curves has been observed also in the previous study [28]. In the report, some clear ferromagnetic hysteresis loops have also been observed below 4.0 K. Also in the present work, we confirmed ferromagnetic hysteresis loops by applying magnetic field along the easy magnetization axis ($\boldsymbol{H}//\boldsymbol{c}$) at 1.9 K and 3.5 K. Figure 4 shows the magnetization as a function of magnetic field, $M(H)$ curves. All the curves show the gentle slope in the initial process from zero magnetic field and steeper rising around 3 kOe. Here, the initial magnetization process is shown only for the $M(H)$ curve at 1.9 K. Both curves tend to saturate at higher magnetic field of 8 kOe and the value at 10 kOe in the isotherm of 1.9 K is 0.08 μ_B.

Therefore, it has been considered that α-Sm_2S_3 is in the WFM state in the temperature region below 4.0 K. And we considered that the sharp peaks around 4.5 K in the ZFC curves are not caused by the magnetic phase transition, because obvious peak has been found in the $C(T)$ curve not at 4.5 K but at 3.6 K, which will be discussed in Section 3.3. It suggests that

the magnetic phase transition occurred at 3.6 K near the shoulders which are observed in the FC curves. Furthermore, the increase of the FC magnetization with decreasing temperature below 3.8 K is also considered to be brought about by the WFM transition because the sharp peak has been found in the $C(T)$ curve at 1.8 K.

So, what caused the sharp peaks in the ZFC curves near 4.5 K for a single crystal? In this regard, we have a simple assumption. Since the sample of a single crystal was cooled down in the presence of a magnetic field for the FC process, the net moments consisting of the short-range order of each Sm^{3+} moment, tend to align along the direction of the external magnetic field. Thus, the FC magnetization keeps rising with decreasing temperature along the direction of the magnetic field down to T_{C1} = 3.6 K. In the case of the ZFC process, $M(T)$ is measured in a heating process. A single crystal was cooled down in the absence of a magnetic field to the lowest measuring temperature (2 K) then the magnetic field of 100 Oe was applied for the first time. In this situation, magnetic domains were formed in the sample to lower magnetostatic energy at sufficiently low temperatures. Hence, the value of net magnetization is so small. However, long-range order disappeared at T_{C1} while heating and then the magnetic domains became unstable. Thus, net moments consisting of short-range order started to orient to the magnetic field. Above the temperature of about 4.5 K, the magnetization turned to decrease with fading out of short-range order.

Next, let us see the $M(T)$ curves of sintered sample. Figure 3(d) shows the $M(T)$ curves for a sintered sample of α-Sm_2S_3 in an applied magnetic field of 100 Oe. Both M-T curves of FC/ZFC show almost the same maxima at 4.0 K and a small separation only below 3.6 K which corresponds to T_{C1}. The increase of magnetization while cooling above 4.0 K is too small compared to the case of the single crystal, and the magnetic phase seems to be paramagnetic with growing short-range order. It is considered that net moments consisting of the short-range order of each Sm^{3+} appear around 4.0 K. The direction of the net moments might be restricted along crystal axes, and the ***c***-axis is the most preferable because of strong anisotropy. As a result, the net moments in various

crystal grain are oriented in random directions. Therefore, the magnetization decreases below 4.0 K. In the process of ZFC, the situation is the same as that of the single crystal. A simple schematic diagram is

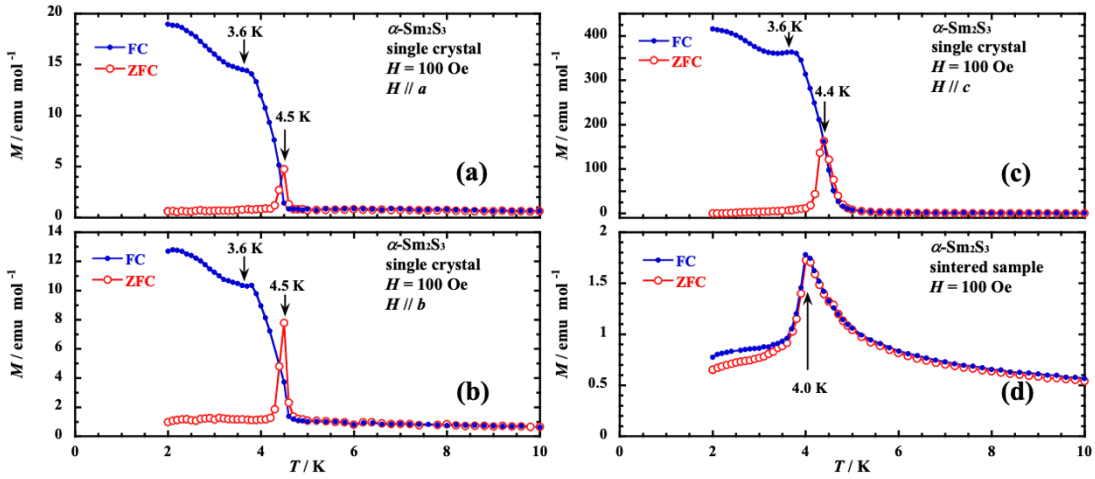

shown in Fig. 5, where the red and blue arrows represent net moments and net magnetization in each crystal grain.

Fig. 3 The $M(T)$ curves for a single crystal and a sintered sample in an applied magnetic field of 100 Oe. The magnetic field is along (a) a-axis; (b) b-axis; (c) c-axis for the single crystal. The figure (d) shows the curves for the sintered sample.

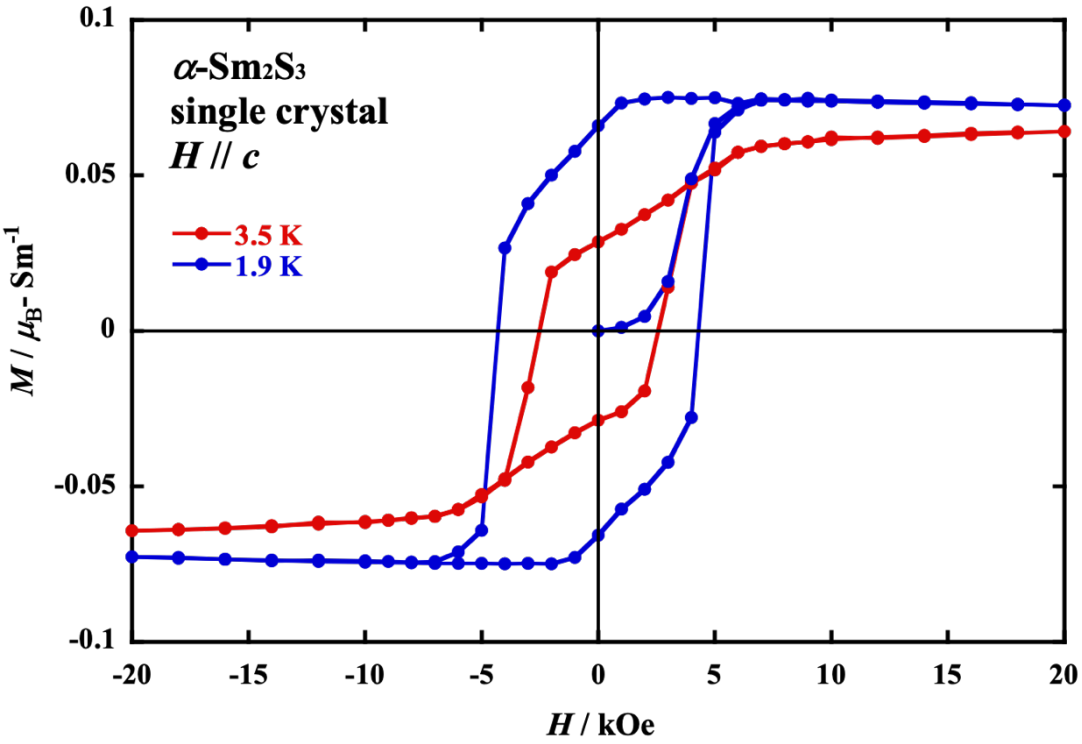

Fig. 4 The magnetization curves at 1.9 K and 3.5 K as a function of magnetic field.

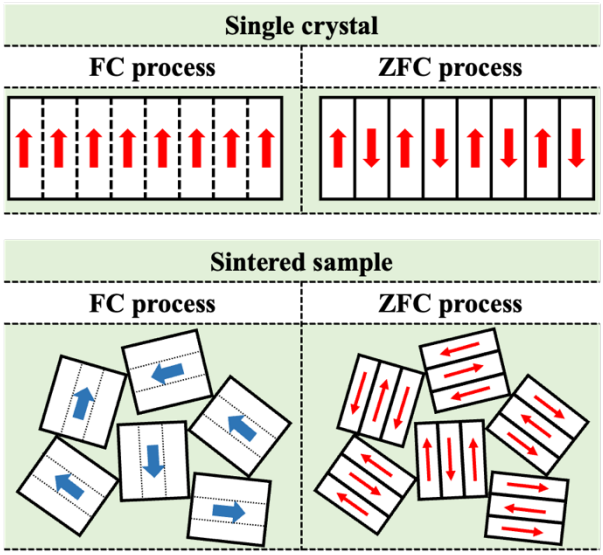

Fig. 5 Schematic diagram of the net moments in a single crystal along the *c*-axis represented by red arrows and net magnetization in each crystal grain in a sintered sample represented by blue arrows.

Next, we show the magnetic field effect on the $M(T)$ curves for both in a single crystal and a sintered sample. Figure 6 shows the $M(T)$ curves for the single crystal of α-Sm_2S_3 in various magnetic fields within 20 kOe along the ***c***-axis. As for the case of $\boldsymbol{H}$ = 1 kOe, the sharp peak in the ZFC curve and the separation between the FC/ZFC curves are clearly seen as well as the case of $\boldsymbol{H}$ = 100 Oe. The peak in the ZFC shifts toward lower temperature, and the saturated value of $M(T)$ at 2.0 K is slightly larger than the value for $\boldsymbol{H}$ = 100 Oe. Such phenomena are not observed under the magnetic field of 10 kOe or stronger. All the FC curves have a tendency of saturation at lower temperatures. However, the features of $M(T)$ under the field of $\boldsymbol{H} \geq$ 10 kOe are obviously different from the curves for $\boldsymbol{H} \leq$ 1 kOe. The former curves indicate a forcibly aligned ferromagnetic state by a magnetic field. Therefore, we cannot see clear shoulders indicating spontaneous ordering in these curves. The saturated values in the FC curves are larger than the corresponding values in the $M(H)$ curve at 1.9 K measured after ZFC process. Moreover, the increasing trend with increasing the magnetic field is not monotonically. It might result from the difference of ordering processes, namely, spontaneous ordering occurred successively in Sm1 and Sm2 sites and forcible ordering occurred

continuously among Sm1 and Sm2. In this way, the value of magnetization is highly dependent on how the magnetic field and temperature are changed. It is considered that such complicated features are brought about by the

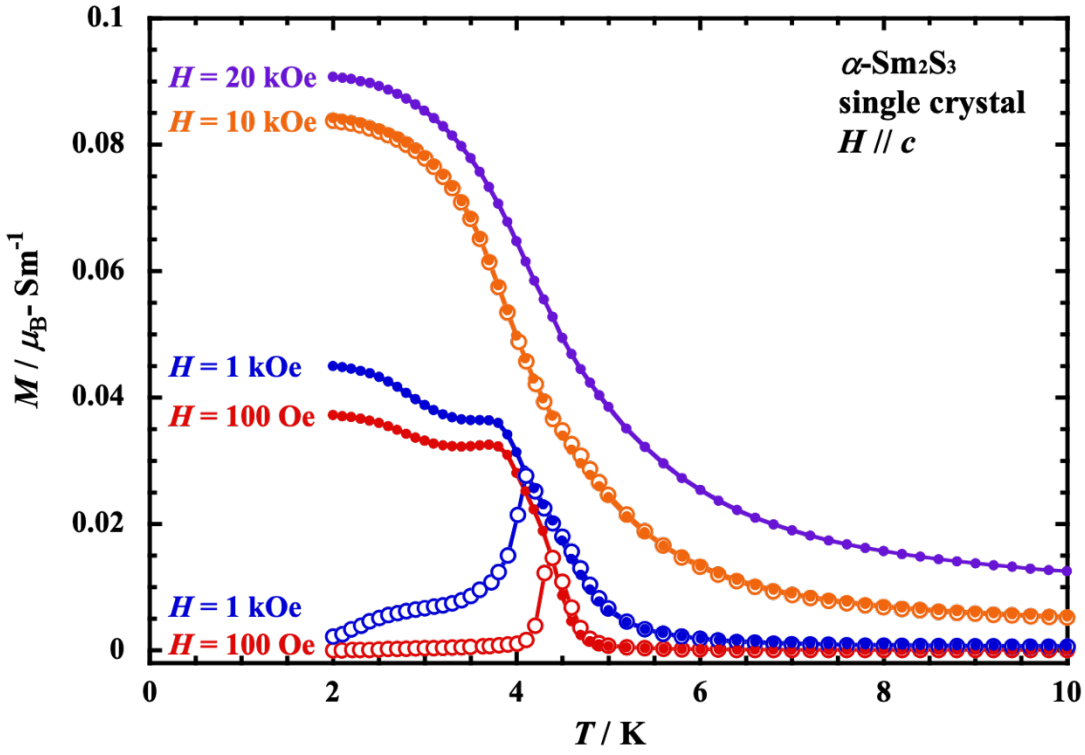

existence of some metastable states.

Fig. 6 The $M(T)$ curves for single crystal of α-Sm_2S_3 in various magnetic fields within 20 kOe along the c-axis.

Figure 7 shows the $M(T)$ curves for the single crystal of α-Sm_2S_3 in various magnetic fields within 20 kOe along the ***a***-and ***b***-axes. As for cases of the ***a***-and ***b***-axes, the behavior of $M(T)$ for $\boldsymbol{H} \leq 1$ kOe are similar to the ***c***-axis qualitatively although the $M(T)$ values are very small. The ferromagnetic net moments seem to be tilted toward ***a*** or ***b*** direction in the relatively weak magnetic field along the ***a***- or ***b***-axis. However, the features of $M(T)$ under the field of $\boldsymbol{H} \geq 10$ kOe are obviously different from the curves for the ***c***-axis. The separation of FC/ZFC curves still exists under the magnetic field of 10 kOe. Because the value of the net moments is not so large in these cases, magnetic domains might remain without annihilation up to higher field than the case of ***H***//***c***. The FC curves do not show the tendency of saturation with decreasing temperature down to 2 K at $\boldsymbol{H} \geq 10$ kOe in both cases. The magnetization along the ***a***-axis, M_a, shows

a broad peak at T_{C1} and tends to decrease with decreasing temperature. In the situation of strong magnetic fields along the ***a***-axis, antiferromagnetically ordered state along the ***b***-axis is considered to be stabilized and the ferromagnetic net moments might be disappeared. On the other hand, the M_b curves along the ***b***-axis show the shoulders near 4 K, and then gentle rising down to 2.4 K, finally turn to decrease with decreasing temperature. In this case, net moments keep existing even in the magnetic field of 20 kOe and tilt toward ***b*** direction slightly. Gentle increase below 4 K might be caused by tilting of each Sm^{3+} moments ordered antiferromagnetically Sm1 site. As for decrease below 2.4 K, we cannot explain enough from only the present data. For each case of the direction of magnetic field, the behavior of Sm2 moments is considered to affect magnetization complicatedly.

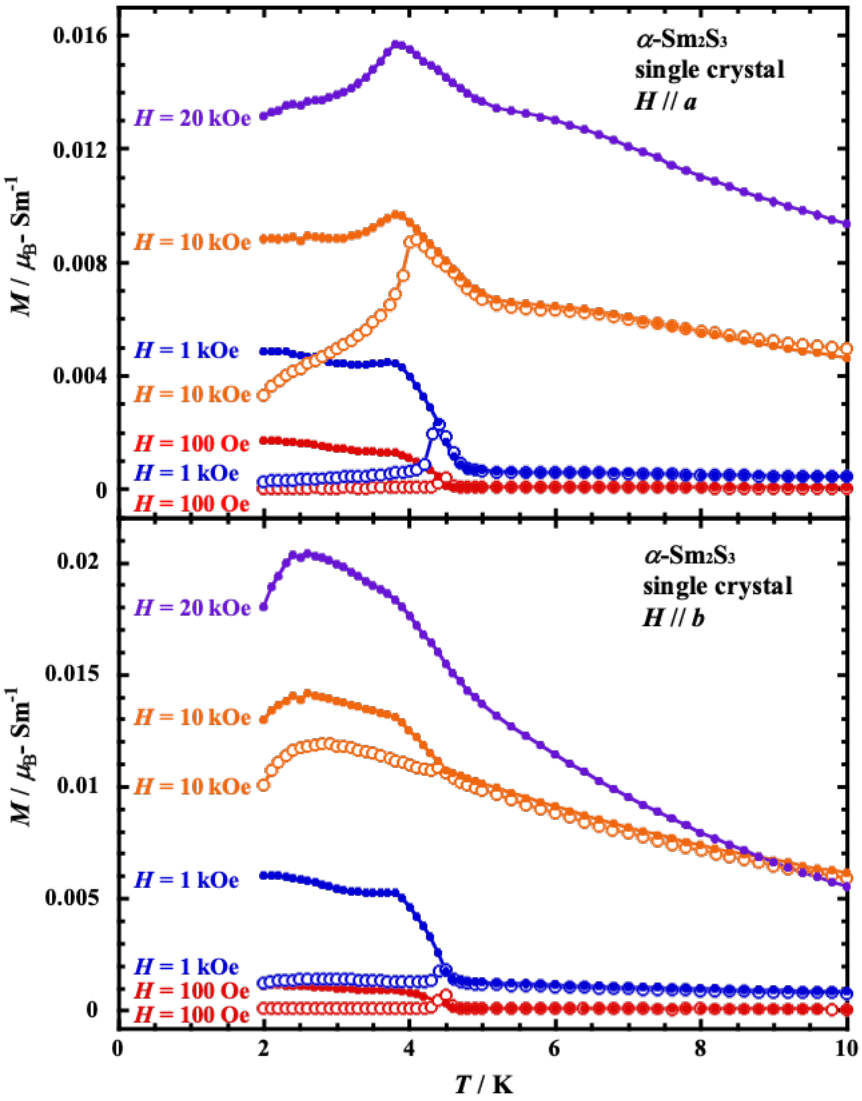

Fig. 7 The $M(T)$ curves for single crystal of α-Sm_2S_3 in various magnetic fields within 20 kOe along the a- and b-axes.

Figure 8 shows the $M(T)$ curves for the sintered sample of α-Sm_2S_3 in various magnetic fields within 70 kOe. Although the separations between FC/ZFC curves are seen in below T_{C1} only in weak magnetic fields of 100 Oe and 1 kOe, they are very small. The peaks around 4 K are observed in the curves for $\boldsymbol{H} \leq 10$ kOe and forcible ferromagnetic states are observed in the curves for $\boldsymbol{H} \geq 20$ kOe. In the FC process, magnetic domains in a small crystal grain must be broken by even a small magnetic field of 100 Oe considering from the result of $M(T)$ for single crystal. However, because of strong magnetic anisotropy the peak keeps existing in 10 kOe.

The magnitude of 20 kOe is required to overcome this strong magnetic anisotropy.

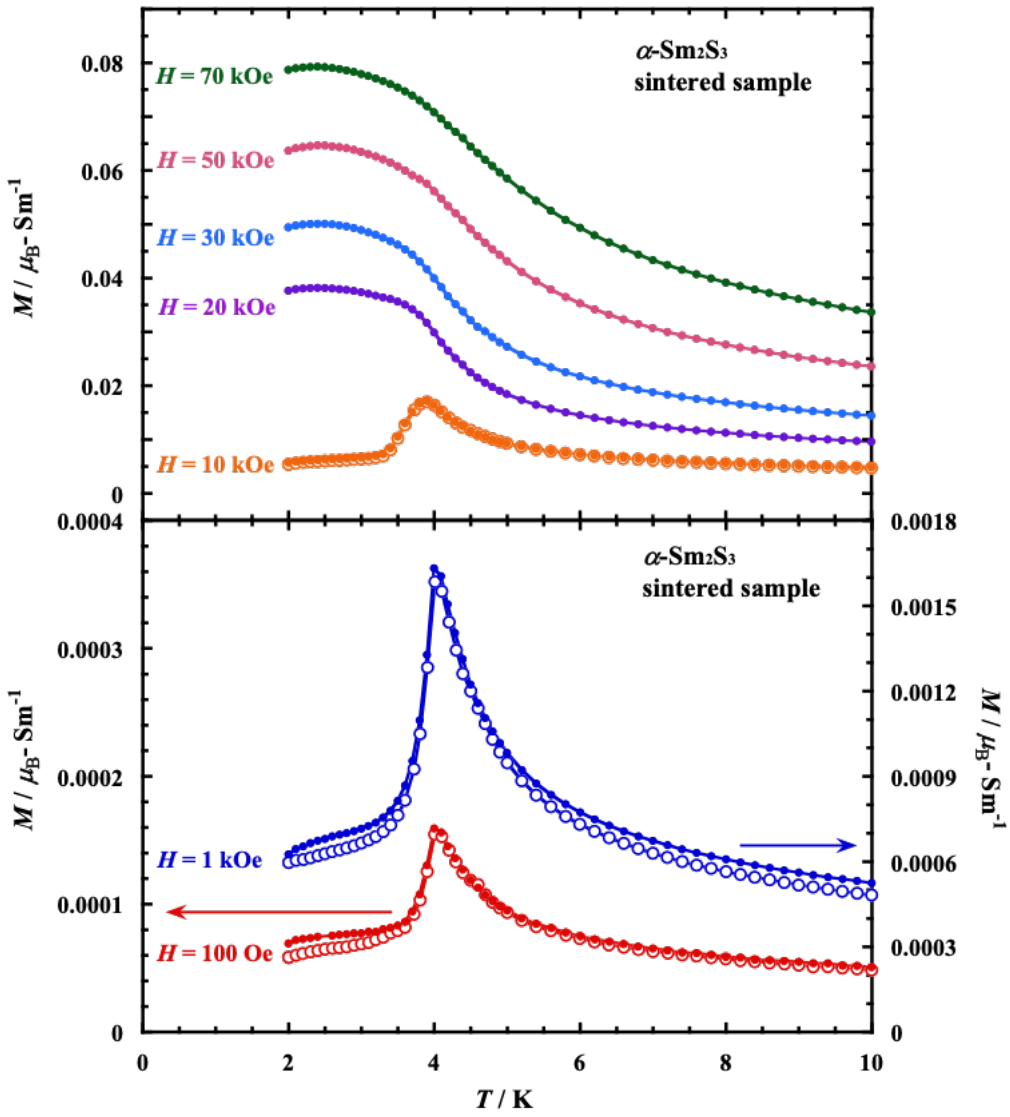

Fig. 8 The $M(T)$ curves for the sintered sample in various magnetic fields within 70 kOe.

3.3 Specific heat

Figure 9 shows the temperature dependence of the molar specific heat for sintered sample of α-Sm_2S_3 measured without applying magnetic field at the wide temperature range from 0.4 K to 300 K. The all plots in the figure are the total experimental specific heat C_p measured. The lattice specific heat C_{lat} was estimated by fitting experimental data to the Debye model, which can be expressed by the following equation:

$$C_{\mathrm{lat}} = 9rN_{\mathrm{A}}k_{\mathrm{B}}\left(\frac{T}{\Theta_{\mathrm{D}}}\right)^{3}\int_{0}^{\frac{\Theta_{\mathrm{D}}}{T}}\frac{x^{4}e^{x}}{(e^{x}-1)^{2}}dx \qquad (1)$$

where, r is number of atoms in the chemical formula unit; N_{A} is the Avogadro constant and k_{B} is the Boltzmann constant. For α-Sm_2S_3, the Debye temperature Θ_{D} estimated here is 325 K, which is very close to the value 317 K for the non-magnetic compound α-La_2S_3 [1] having the same crystal structure. At 300 K, C_{lat} reaches a value of about 120 J K^{-1} mol^{-1}, which is close to the Dulong-Petit limiting value of $3rR$ = 125 J K^{-1} mol^{-1} (where, r = 5 for α-Sm_2S_3 and R is the gas constant). In low temperature range, two sharp peaks are observed at 3.75 K and 1.85 K, as shown in the inset of Fig. 9.

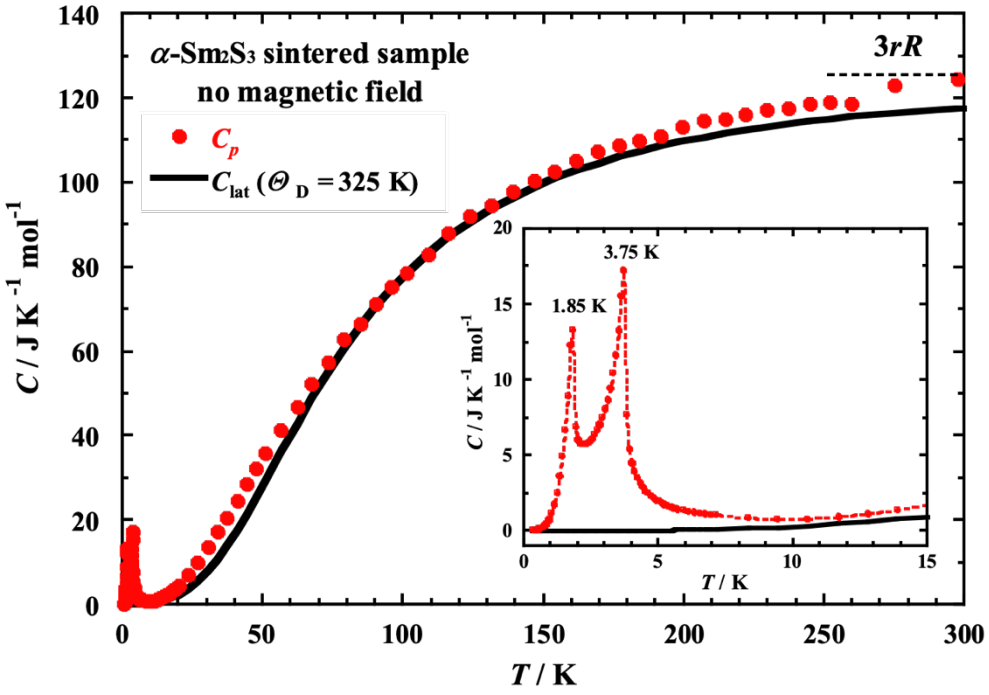

Fig. 9 Temperature dependence of the molar specific heat for sintered sample of α-Sm_2S_3 measured in no magnetic field at the wide temperature range from 0.4 K to 300 K.

Figure 10 shows the temperature dependence of the magnetic molar specific heat; C_{mag} and the magnetic entropy per mol-Sm; S_{mag} in no magnetic field for both a single crystal and a sintered sample of α-Sm_2S_3. Since the electrical properties of the α-Sm_2S_3 compound is not metallic at lower temperature range [28, 29], only the lattice contribution C_{lat} and the magnetic contribution C_{mag} are considered for the specific heat C_p. Thus,

the magnetic part of specific heat C_{mag} is obtained by subtracting the lattice specific heat C_{lat} from the total specific heat C_p. The magnetic entropy $S_{mag}(T)$ for mol-Sm was calculated by following equation:

$$S_{\mathrm{mag}}(T) = \int_{T_0}^{T} \frac{C_{\mathrm{mag}}}{nT}\, dT \qquad (2)$$

where T_0 is the lowest temperature of about 0.36 K, $n = 2$ is the number of Sm atoms in formula unit. Because the $C_{mag}(T_0)$ is close to 0 and $C_{mag}(T)$ shows a tendency to approach 0 with decreasing temperature from T_0, we considered the S_{mag} below T_0 is negligible.

As shown in Fig. 10, a clear double-peak is observed in both curves for a single crystal and a sintered sample. These peaks must show ferromagnetic transitions because we have seen increasing of magnetization at corresponding temperatures. We have determined the Curie temperatures as $T_{C1} = 3.6$ K and $T_{C2} = 1.8$ K from the temperatures at which the C_{mag} for the single crystal have maxima of the peaks. It seems somewhat strange that the temperatures of peak maxima for the sintered sample are slightly higher than those for the single crystal. The magnetic entropy changes per mol-Sm, S_{mag}, across each magnetic transition are estimated as nearly (Rln2)/2. It reveals that the magnetic moments only on one Sm site are ordered at each transition temperature and the ground state of Sm^{3+} on each Sm site is a doublet. Kramer's degeneracy must remain under crystalline electric field since Sm^{3+} has 5 electrons (odd numbers) in the 4f orbital. Thus, it seems reasonable that one of the Kramer's doublets is the ground term of Sm^{3+} in the present crystal structure having low symmetry. Similar results were found in the Dy^{3+} having $4f^9$ configuration [22] and Nd^{3+} having $4f^3$ configuration [13]. We should point out the peak of T_{C1} for the single crystal is lower and broader than that for the sintered sample surprisingly, while a rattling phenomenon appears at the bottom of the curve between the successive transitions for the single crystal. Although we cannot specify the reason of this rattling, this might be bringing about the error of overestimation of the magnetic entropy slightly larger than Rln2 at $T > 6$ K.

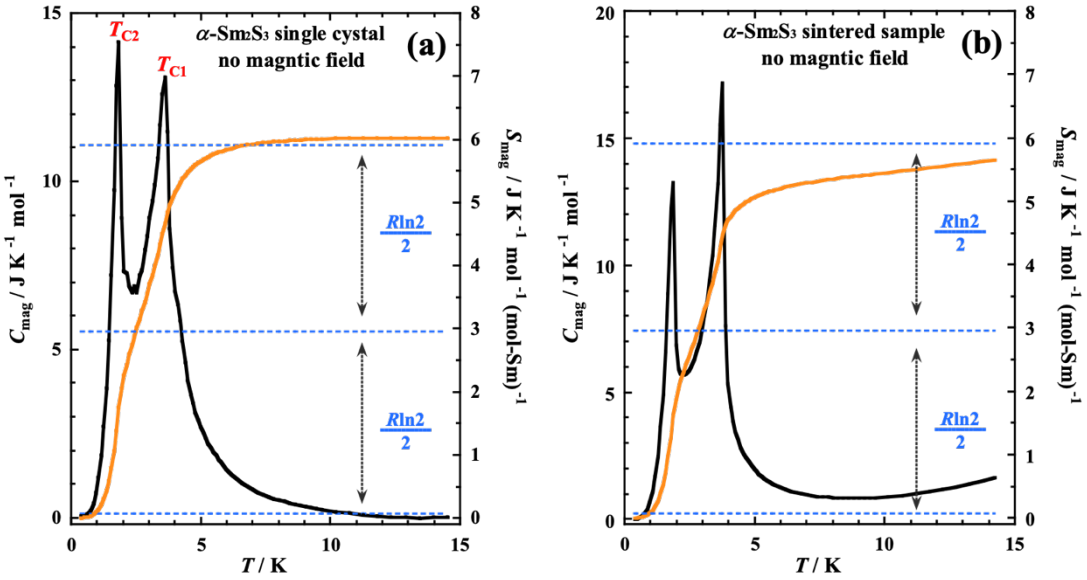

Fig. 10 Temperature dependence of the magnetic molar specific heat C_{mag} and the magnetic entropy per mol-Sm S_{mag} in no magnetic field for (a) a single crystal and (b) a sintered sample of α-Sm_2S_3.

Figure 11 shows the temperature dependence of the magnetic molar specific heat C_{mag} in various magnetic fields within 70 kOe for the single crystal and the sintered sample of α-Sm_2S_3. For the single crystal in zero magnetic field, two peaks are observed at T_{C1} = 3.6 K and T_{C2} = 1.8 K. While increasing the magnetic field parallel to the ***a***-axis, the T_{C1} peak keeps constant for the magnitude and the maximum temperature up to $\boldsymbol{H}$ = 20 kOe, then the maximum value gradually decreases and the peak shifts slightly toward lower temperature from $\boldsymbol{H}$ = 30 kOe. On the other hand, the T_{C2} peak is enhanced and shifts slightly toward lower temperature with the increase of the magnetic field. Under the magnetic field parallel to the ***b***-axis, both T_{C1} and T_{C2} peaks shift toward lower temperature and the maximum values of the two peaks reduced by increasing the magnetic field. Especially, the features are marked for the T_{C2} peak at $\boldsymbol{H} \geq$ 30 kOe. Contrary, in the case of the ***c***-axis, T_{C1} peak shifts toward higher temperature meanwhile the maximum value of the peak reduces obviously, and the peak of this transition became broader with increase of the magnetic field. As for the T_{C2} peak, it does not shift at all while increasing the magnetic field, but it shows a large enhancement at $\boldsymbol{H}$ = 10 kOe and keeps the values up to 70 kOe. As for the sintered sample, unlike the single

crystal, neither the two peaks have a significant shift, however, those maximum values decrease clearly with increasing the magnetic field.

From the consideration of the crystal structure and the neutron diffraction result for α-Tb_2S_3 [25], it might be natural that the Sm1 site moments order at T_{C1} and the Sm2 site moments order at T_{C2}. The shift of the peak of T_{C1} toward higher temperature in Fig. 11(c) demonstrates a preference of Sm1 moments for directing along the ***c***-axis. It is consistent with the easy magnetization axis seen in the magnetic measurements. The broadening of the peak means that the weak ferromagnetic alignment is made forcibly by a strong magnetic field. The shift of the peak at T_{C2} toward lower temperature in Fig. 11(b) suggests the Sm2 moments basically align along the ***b***-axis antiferromagnetically. Canting of these antiferromagnetically ordered moments are considered to contribute to weak ferromagnetic features.

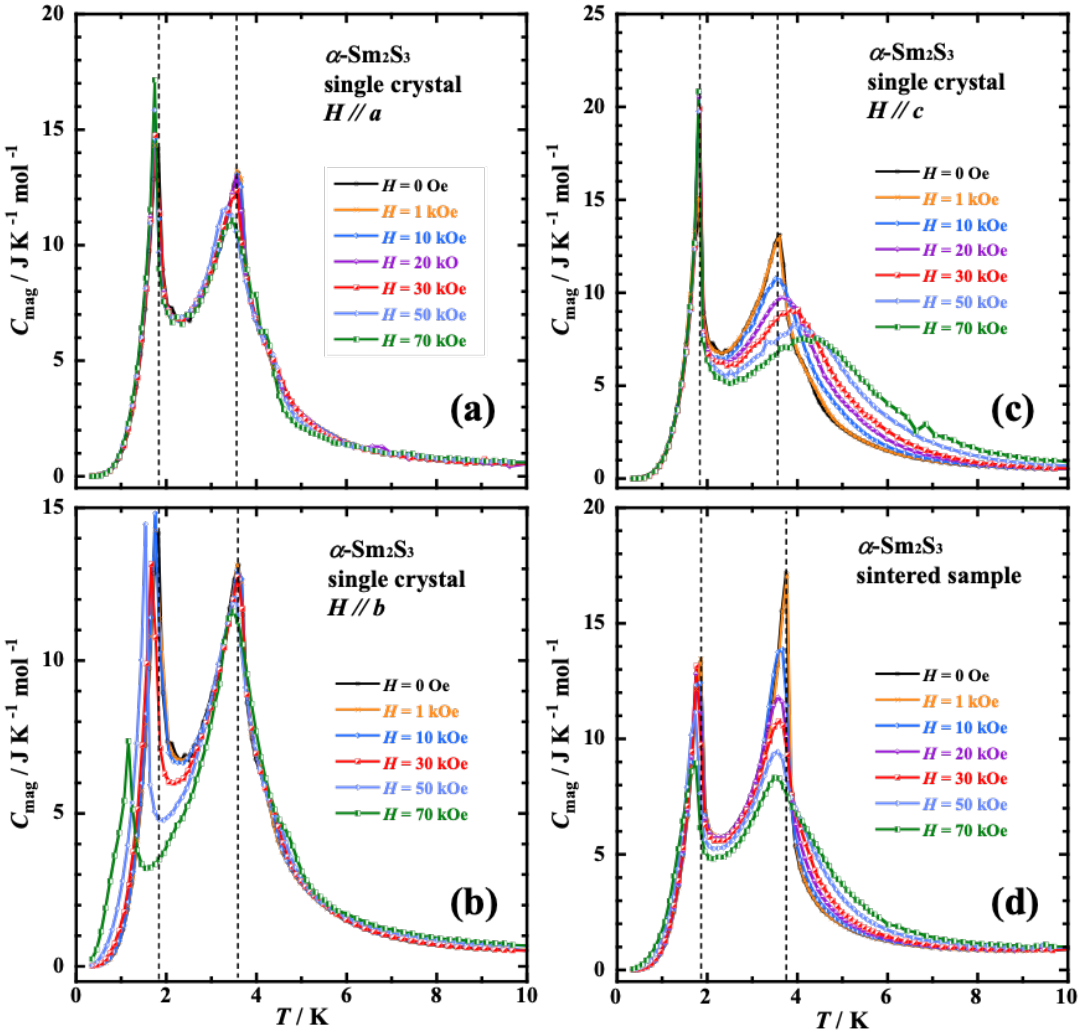

Fig. 11 Temperature dependence of the magnetic molar specific heat C_{mag} in various magnetic fields within 70 kOe. The magnetic field is along (a) *a*-axis; (b) *b*-axis; (c) *c*-axis for the single crystal. The figure (d) shows the curves for the sintered sample.

Figure 12 shows the temperature dependence of the magnetic entropy per mol S_{mag} in various magnetic fields within 70 kOe for the single crystal. We can see obvious changes of S_{mag} at the higher temperature than T_{C1} in Fig. 12(c) and at the lower temperature than T_{C2} in Fig. 12(b). These features reflect well the characteristics of the temperature dependence of the specific heat $C_{mag}(T)$ in Fig. 11(c) and Fig. 11(b). In order to see the magnetic entropy change directly by the magnetic field, we have calculated the value of $-\Delta S_{mag}(T, H)$ using the following equation:

$$-\Delta S_{mag}(T, H) = - [S_{mag}(T, H) - S_{mag}(T, 0)]. \quad (3)$$

The values for the cases of ***H*//*b*** and ***H*//*c*** are plotted versus temperature in the insets of Fig. 12(b) and Fig. 12(c), respectively. As shown in the inset of Fig. 12(c), the maximum magnetic entropy changes -ΔS_{mag}'s are seen near the transition temperature T_{C1}. With the increase of the magnetic field, the absolute value of the -ΔS_{mag} increases gradually, but the values are relatively small. The maximum value of -ΔS_{mag} is about 4.1 J kg^{-1} K^{-1} at 4.0 K in 70 kOe, which is as small as 1/7 of α-Dy_2S_3 in the case of ***H*⊥*b*** (***H*** = 50 kOe) [27]. As for the case of ***H*//*b***, the value of -ΔS_{mag} around T_{C2} in the magnetic field stronger than 10 kOe is negative, interestingly. It should be pointed out that the curve of magnetic entropy $S_{mag}(T)$ for the case of ***H*//*a*** is almost the same within the magnetic field of 70 kOe. This is an interesting feature unique to the present compound α-Sm_2S_3 having a strong anisotropy. Although the magnetocaloric effect (MCE) is not large even in the case of ***H*//*c***, it might be expected to use for MCE device controllable by changing the orientation of single crystal under a magnetic field.

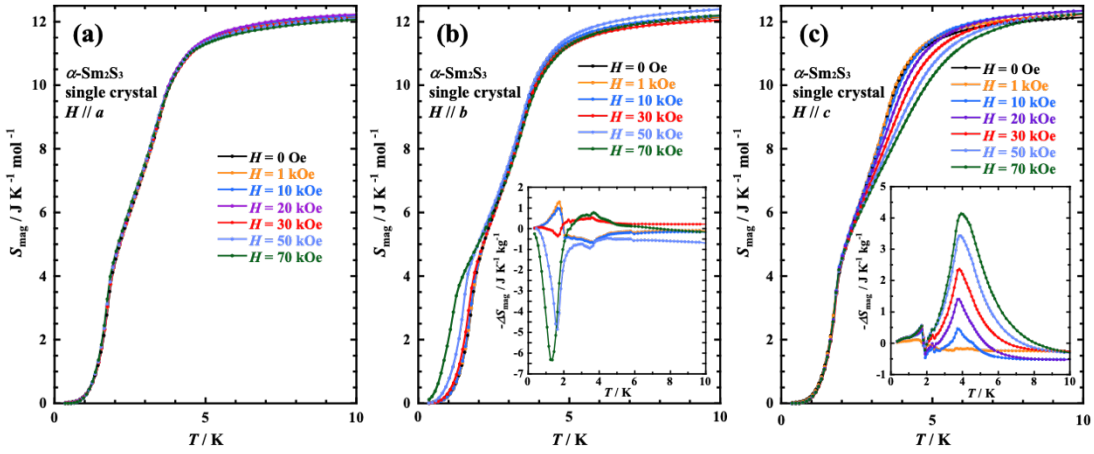

Fig. 12 The temperature dependence of magnetic entropy per mol S_{mag} in various magnetic fields along (a) *a*-axis; (b) *b*-axis; (c) *c*-axis. The insets in (b) and (c) show the temperature dependence of magnetic entropy change -$\Delta S_{mag}(T, H)$ for each case.

4. Conclusion

In this work, the temperature dependence of magnetization and specific heat were investigated using a single crystal and a sintered sample of α-Sm_2S_3. The magnitude of the magnetization is extremely anisotropic, and the easy-magnetization axis is ***c*** for the single crystal used. However,

features of successive weak-ferromagnetic transitions have been observed commonly in the FC $M(T)$ curves under the weak magnetic field $H \leq 1$ kOe along each crystal axis for the single crystal. All the ZFC $M(T)$ curves for the single crystal and both the FC/ZFC $M(T)$ curves for the sintered sample demonstrate characteristic sharp peaks at 4.0-4.5 K near higher WFM transition temperature. The successive WFM transitions have been confirmed as the sharp peaks in the temperature dependence of specific heat. We have determined the Curie temperatures as $T_{C1} = 3.6$ K and $T_{C2} = 1.8$ K from the magnetic specific heat $C_{mag}(T)$ of a single crystal under no magnetic field. We have considered that the sharp peaks in the ZFC $M(T)$ which emerge at slightly higher temperature than T_{C1} are basically caused by the formation of magnetic domains. While the sharp peak in the FC $M(T)$ of the sintered sample has been considered to be result from strong anisotropy of α-Sm_2S_3 and existence of crystal domains in the sintered sample. By evaluating the magnetic entropy in no magnetic field across the transitions, we have found that the ground state of Sm^{3+} on each Sm site is a doublet. Moreover, we have assumed the Sm1 moments order at T_{C1} and the Sm2 moments order at T_{C2} by analogy with the results of neutron diffraction measurement on α-Tb_2S_3 [25]. Novel magnetic field dependence of the specific-heat peak has been found. The T_{C1} peak shifts toward higher temperature with increasing magnetic field only when the magnetic field is applied along the ***c***-axis. The shift is accompanied by broadening of the peaks. On the other hand, the T_{C2} peak shifts toward lower temperature only under the magnetic field along the ***b***-axis with keeping its sharpness. Both peaks under the magnetic field along the ***a***-axis do not show much change. We concluded that the shifts of the T_{C1} peak toward higher temperature suggests a preference of the net moments consisting of Sm1 moments for directing along the ***c***-axis. The broadening of the peak means that the weak ferromagnetic alignment is made forcibly by a strong magnetic field. The shifts of the T_{C2} peak to low temperature side suggests the Sm2 moments prefer to align along the ***b***-axis antiferromagnetically. We hope that our speculation will be validated by some microscopic measurements. Such anisotropic features in the magnetic specific heat are reflected on the magnetic entropy change. The

largest magnetic entropy change is brought about near T_{C1} by applying magnetic field along the ***c***-axis, although the magnitude is not as large as the other MCE materials. However, the magnetic entropy $S_{mag}(T)$ of α-Sm_2S_3 is extremely anisotropic, and the $S_{mag}(T)$ under the magnetic field along the ***a***-axis is almost invariant to the field within 70 kOe. Therefore, the single crystal of α-Sm_2S_3 might be useable for controlling MCE effect by its rotating in magnetic field.

Acknowledgment

The authors would like to thank Prof. Ishigaki in Ibaraki Univ. for valuable discussion about the crystal structure. This work was supported by JSPS KAKENHI, Grant No. 19K05238 and JST Spring, Grant No. JPMJSP2153.

References

[1] K. A. Gschneidner, Jr., B. J. Beaudry, T. Takeshita, S. S. Eucker, Low-temperature heat capacities of yttrium, lanthanum, and lutetium sesquisulfides, Phys. Rev. B, 24 (1981) 7187-7193, https://doi.org/10.1103/physrevb.24.7187

[2] J. Ho, S. Taher, G. King, J. Gruber, B. Beaudry, K. Gschneidner, Jr, Heat capacity of rare earth sesquisulfides, J. Phys. Col., 39 (1978) C6-840-C6-842, https://doi.org/10.1051/jphyscol:19786374

[3] H. L. Beeler, J. B. Gruber, Average magnetic susceptibility of rare earth sesquisulfides, Chem. Phys., 13 (1976) 359-362, https://doi.org/10.1016/0301-0104(76)87005-X

[4] J. R. Henderson, M. Muramoto, E. Loh, J. B. Gruber, Electronic structure of rare-earth sesquisulfide crystals, J. Chem. Phys., 47 (1967) 3347-3356, https://doi.org/10.1063/1.1712397

[5] S. M. Taher, J. B. Gruber, Thermoelectric efficiency of rare earth sesquisulfides, Mat. Res. Bull., 16 (1981) 1407-1412, https://doi.org/10.1016/0025-5408(81)90060-X

[6] C. R. Wang, Y. Y. Chen, Y. D. Yao, Y. S. Lin, M. N. Ou, S. M. A. Taher, H. H. Hamdeh, X. Zhang, J. C. Ho, J. B. Gruber, Magnetic and calorimetric studies of antiferromagnetic transitions in erbium sesquisulfide, J. Magn. Magn. Mater., 269 (2004) 419-422, https://doi.org/10.1016/S0304-8853(03)00653-X

[7] X. X. LUO, M. ZHANG, L. B. MA, Y. PENG, Preparation and stabilization of γ-La_2S_3 at low temperature, J. Rare Earths, 29 (2011) 313-316, https://doi.org/10.1016/S1002-0721(10)60450-4

[8] A. A. Kamarzin, K. E. Mironov, V. V. Sokolov, Yu. N. Malovitsky, I. G. Vasil'yeva, Growth and properties of lanthanum and rare-earth metal sesquisulfide crystals, J. Cryst. Growth, 52 (1981) 619-622, https://doi.org/10.1016/0022-0248(81)90351-1

[9] S. M. A. Taher, A. Braun, J. L. Schwartz, J. B. Gruber, Electrical resistivity in metallic rare earth sesquisulfides, J. Less-Common Met., 111 (1985) 361-368, https://doi.org/10.1016/0022-5088(85)90211-5

[10] M. Kanazawa, L. Li, T. Kuzuya, K. Takeda, S. Hirai, Y. Higo, T. Shinmei, T. Irifune, C. Sekinea, High-pressure and high-temperature synthesis of heavy lanthanide sesquisulfides Ln_2S_3 (*Ln*=Yb and Lu), J. Alloys Compd., 736 (2018) 314-321, https://doi.org/10.1016/j.jallcom.2017.11.090

[11] Y. Chen, L. Li, S. Hirai, Fabrication, sintering, heat capacity, magnetic and magneto-resistivity properties of ytterbium sulfides, J. Magn. Magn. Mater., 476 (2019) 289-296, https://doi.org/10.1016/j.jmmm.2018.12.100

[12] R. Windiks, E. Wimmer, L. Pourovskii, S. Biermann, A. Georges, Structure and optical properties of α- and γ-cerium sesquisulfide, J. Alloys Compd., 459 (2008) 438-446, https://doi.org/10.1016/j.jallcom.2007.04.306

[13] S. Ebisu, T. Nagata, K. Fuji, Y. Shibayama, Magnesium in α-R_2S_3 (*R*= Pr and Nd) single crystals, J. Phys.: Conf. Ser. 568 (2014) 042003, https://doi.org/10.1088/1742-6596/568/4/042003

[14] S. Ebisu, Y. Iijima, T. Iwasa, S. Nagata, Antiferromagnetic transition and electrical conductivity in α-Gd_2S_3, J. Phys. Chem. Solids 65 (2004) 1113-1120, https://doi.org/10.1016/j.jpcs.2003.12.002

[15] A. Kikkawa, K. Katsumata, S. Ebisu, S. Nagata, Phase transition of a frustrated magnet α-Gd_2S_3, J. Phys. Soc. Japan, 73 (2004) 2955-2958, https://doi.org/10.1143/JPSJ.73.2955

[16] K. Katsumata, A. Kikkawa, Y. Tanaka, S. Shimomura, S. Ebisu, S. Nagata, Synchrotron X-ray diffraction studies of α-Gd_2S_3, J. Phys. Soc. Japan, 74 (2005) 1598-1601, https://doi.org/10.1143/JPSJ.74.1598

[17] M. Matsuda, A. Kikkawa, K. Katsumata, S. Ebisu, S. Nagata, Neutron diffraction study of α-Gd_2S_3, J. Phys. Soc. Japan 74 (2005) 1412-1415, https://doi.org/10.1143/JPSJ.74.1412

[18] L. E. Roy, T. Hughbanks, Tight binding prediction of the α-Gd_2S_3 magnetic structure, J. Solid State Chem., 180 (2007) 818-823, https://doi.org/10.1016/j.jssc.2006.11.035

[19] S. Ebisu, M. Narumi, S. Nagata, Anomalous enlargement of electrical resistivity between successive magnetic transitions in α-Dy_2S_3, J. Phys. Soc. Japan 75 (2006) 085002, https://doi.org/10.1143/JPSJ.75.085002

[20] S. Ebisu, M. Narumi, M. Gorai, S. Nagata, Successive magnetic phase transitions in α-Dy_2S_3 single crystal, J. Magn. Magn. Mater., 310 (2007) 1741-1743, https://doi.org/10.1016/jmmm.2006.10.571

[21] S. Ebisu, K. Koyama, T. Horikoshi, M. Kokita, S. Nagata, Extremely broad hysteresis in the magnetization process of α-Dy_2S_3 single crystal induced by high field cooling, J. Phys.: Conf. Ser. 400 (2012) 032010, https://doi.org/10.1088/1742-6596/400/3/032010

[22] S. Ebisu, Y. Ushiki, S. Takahashi, Specific-heat study on successive magnetic transitions in α-Dy_2S_3 single crystals under magnetic fields, J. Kor. Phys. Soc. 63 (2013) 571, https://doi.org/10.3938/jkps.63.571

[23] S. Ebisu, K. Fuji, Q. Qing, M. Miyazaki, Metastable magnetic phase induced by rotation of α-Dy_2S_3 single crystal in magnetic field, J. Magn. Magn. Mater., 444 (2017) 140-145, https://doi.org/10.1016/jmmm.2017.08.018

[24] S. Ebisu, M. Gorai, K. Meakawa, S. Nagata, Highly anisotropic properties of an antiferromagnetic α-Tb_2S_3 single crystal, AIP Conf. Proc. **850** (2006) 1237, https://doi.org/10.1063/1.2355152

[25] M. Matsuda, K. Kakurai, S. Ebisu, S. Nagata, Successive magnetic phase transitions in α-Tb_2S_3 studied by neutron diffraction technique, J. Phys. Soc. Japan 75 (2006) 074710, https://doi.org/10.1143/JPSJ.75.074710

[26] S. Ebisu, K. Koyama, H. Omote, S. Nagata, High field magnetization processes in single crystals of α-Tb_2S_3 and α-Dy_2S_3, J. Phys.: Conf. Ser. 150 (2009) 042027, https://doi.org/10.1088/1742-6596/150/4/042027

[27] Q. Guo, O. Tegus, S. Ebisu, Specific heat in magnetic field and magnetocaloric effects of α-R_2S_3 (R= Tb, Dy) single crystals, J. Magn. Magn. Mater., 465 (2018) 260-269, https://doi.org/10.1016/jmmm.2018.05.072

[28] S. Ebisu, H. Omote, S. Nagata, Drastic change of the electrical resistivity related to the novel magnetic phase transition in α-Sm_2S_3, J. Phys.: Conf. Ser. 200 (2010) 092005, https://doi.org/10.1088/1742-6596/200/9/092005

[29] S. Ebisu, T. Era, Q. Guo, M. Miyazaki, Extremely anisotropic suppression of huge enhancement of electrical resistivity by magnetic field in α-R_2S_3 (R = Sm, Dy), J. Phys.: Conf. Ser. 969 (2018) 012124, https://doi.org/10.1088/1742-6596/969/1/012124

[30] N. Kijima, K. Morie, S. Chikazawa, H. Nishihara, S. Nagata, Resistance Anomaly in Quasi-One-Dimensional Sulfide $BaNbS_{3+\delta}$, J. Solid State Chem., 142 (1999) 57-62, https://doi.org/10.1006/jssc.1998.7985

[31] P. Peshev, W. Piekarczyk, S. Gazda, The growth of α-Gd_2S_3 single crystals from the gaseous phase and some of their physical properties, Mat. Res. Bull., 6 (1971) 479-486, https://doi.org/10.1016/0025-5408(71)90026-2

[32] V. M. Kovrugin, M. Colmont, O. I. Siidr, V. V. Gurzhiy, S. V. Krivovichev, O. Mentré, Pathways for synthesis of new selenium-containing oxo-compounds: Chemical vapor transport reactions, hydrothermal techniques and evaporation method, J. Cryst. Growth, 457 (2017) 307-313, https://doi.org/10.1016/j.jcrysgro.2016.01.006

[33] P. Kannappan, R. Dhanasekaran, Studies on structural and optical properties of ZnSe and ZnSSe single crystals grown by CVT method, J. Cryst. Growth, 401 (2014) 691-696, https://doi.org/10.1016/j.jcrysgro.2013.11.030